Nano Energy 35 (2017) 350–357

Contents lists available at ScienceDirect

Nano Energy

journal homepage: www.elsevier.com/locate/nanoen

Full paper

The effects of Al substitution and partial dissolution on ultrathin NiFeAl trinary layered double hydroxide nanosheets for oxygen evolution reaction in alkaline solution

Haixia Liu[a,1], Yanrong Wang[a,1], Xinyao Lu[a], Yi Hu[a], Guoyin Zhu[a], Renpeng Chen[a], Lianbo Ma[a], Hongfei Zhu[a], Zuoxiu Tie[b], Jie Liu[a,c], Zhong Jin[a,*]

[a] Key Laboratory of Mesoscopic Chemistry of MOE and Collaborative Innovation Center of Chemistry for Life Sciences, School of Chemistry and Chemical Engineering, Nanjing University, Nanjing 210023, China
[b] College of Engineering and Applied Sciences, Nanjing University, Nanjing, Jiangsu 210093, China
[c] Department of Chemistry, Duke University, Durham, NC 27708, USA

ARTICLE INFO

Keywords:
Trinary layered double hydroxides
Two-dimensional layered materials
Ultrathin nanosheets
Oxygen evolution reaction
Electrocatalysis in alkaline solution

ABSTRACT

Recently, Ni–based layered double hydroxide (LDH) materials have attracted growing interest owing to the remarkable performance for oxygen evolution reaction (OER). Here we demonstrate the preparation of ultrathin Ni_3FeAl_x trinary LDH nanosheets with higher activity and stability than NiFe–LDH nanosheets for OER. The enhancement was derived from Al substitution, which increased the concentration of Ni^{3+} active sites on the catalyst surface. Besides, low-coordinated Ni and Fe atoms and defects were formed by partial etching/dissolution of Al^{3+} in alkaline solution, which further increased the activity towards OER. To improve the conductivity, Ni_3FeAl_x–LDH (x=0, 0.91, 1.27 or 2.73) nanosheets were also *in-situ* grown on three-dimensional-networked nickel foam. The binder-free Ni_3FeAl_x–LDH/Ni foam electrodes exhibited further improved catalytic performance compared to the electrodes made of powdery Ni_3FeAl_x–LDHs and nafion binder. The best OER performance was presented by $Ni_3FeAl_{0.91}$–LDH/Ni foam, showing a Tafel slope of 57 mV/dec, a low overpotential (304 mV) at the current density of 20 mA/cm^2, and a current density of 235 mA/cm^2 at 1.60 V (*vs.* RHE). Furthermore, the $Ni_3FeAl_{0.91}$–LDHs/Ni foam electrode showed excellent long-term stability, maintaining a stable overpotential of 320 mV at 20 mA/cm^2 after testing for 18 h.

1. Introduction

Oxygen evolution reaction (OER) is one of the major bottlenecks in many important energy conversion processes [1–5], such as the water splitting for hydrogen production [6] and the electrochemical reduction of harmful CO_2 emissions [7]. Due to the slow kinetics, normally the overall energy conversion efficiency of OER is significantly limited by the high overpotential. Therefore, effective electrocatalyst is a necessity in most of cases. However, numerous catalysts reported in the literature are usually based on scarce and expensive materials, such as IrO_2 and RuO_2 [8–10]. It is very important to develop high-performance catalysts based on earth-abundant materials with long-term stability under continuous exposure to oxidizing conditions.

The process of OER is determined by the formation and adsorption of intermediate –OOH, and the transport of electrons [11,12]. Transition metal layered double hydroxides (LDHs) have been demonstrated to have good efficiency and anti-corrosion stability for OER in alkaline condition and much lower cost than RuO_2 or IrO_2 based electrocatalysts [13–19]. Besides, ultrathin LDH nanosheets present much higher activity than their counterpart bulky LDHs [14,17,20]. Among the diverse LDH electrocatalysts, NiFe–LDHs have been intensively studied because they are considered as one class of the most active catalysts in alkaline medium [21–26], which exhibit an OER turnover frequency (TOF) > 10 fold higher than that of IrO_x [27]. However, NiFe–LDHs suffer from poor electronic conductivity that hampers their practical application as electrode materials. To overcome this shortage, coupling LDHs with three-dimensional (3D) conductive architectures with superior electron conductivity (such as CNTs [22], nickel foam [28,29], graphene framework [30], defective grapheme [31], exfoliated graphene foil [32]) is a feasible solution that can lead to a dramatic improvement in the electrochemical performance. In brief, 3D porous conductive architectures can offer several critical advan-

* Corresponding author.
E-mail address: zhongjin@nju.edu.cn (Z. Jin).
[1] These two authors contributed equally to this work.

http://dx.doi.org/10.1016/j.nanoen.2017.04.011
Received 14 January 2017; Received in revised form 3 April 2017; Accepted 5 April 2017
Available online 06 April 2017

tages: 1) facilitating electron transport, 2) promoting electrolyte penetration, and 3) increasing electrochemically-active surface area (ECSA).

Previous works [33–35] show that low-coordinated Ni, Fe and Co sites originated from defects or vacancies in disordered or amorphous structures can serve as the active sites for OER catalysis. Therefore, it is promising to further improve the catalytic activity of NiFe–LDHs by increasing the proportion of low-coordinated Ni and Fe sites. Elemental doping has been demonstrated to be an effective approach to adjust the coordination valence states and chemical environment of electrocatalysts [36,37]. Moreover, by the selective etching/dissolution of less stable elements [38], more defects will be created on the surface of electrode and more surface metal atoms with low coordination number will be exposed, so that the surface energy and the number of electrocatalytic sites can be further increased.

Inspired by the above analysis, we propose that the electrocatalytic activity of NiFe–LDHs can be increased by aluminum (Al) substitution, because the introduction of trivalent Al ions will greatly increase the faction of low-coordinated Ni and Fe atoms. Furthermore, the number of active sites will be greatly increased by the etching of Al species in strong alkaline solution, which is expected to be very beneficial to the OER performances in alkaline conditions. Herein, we demonstrate the preparation of rationally-designed ultrathin NiFeAl trinary LDH (Ni_3FeAl_x–LDH) nanosheets, which can be used as remarkable electrocatalysts with superior catalytic activity and stability towards OER. The ultrahigh activity is mainly attributed to the increased concentration of active site Ni^{3+} by the introduction of Al^{3+}. Besides, more exposed active sites/defect sites (*i.e.* Ni^{3+} and Fe^{3+}) formed by partial dissolution of Al^{3+} in strong alkaline solution also play an important role in the enhancement of catalytic activity. Our research shows that $Ni_3FeAl_{0.91}$–LDH nanosheets exhibit highest catalytic activity towards OER when comparing with Ni_3Fe–LDH, $Ni_3FeAl_{1.27}$–LDH and $Ni_3FeAl_{2.73}$–LDH nanosheets. To further improve the conductivity of electrodes, ultrathin Ni_3FeAl_x–LDH nanosheets grown on 3D porous Ni foam (Ni_3FeAl_x–LDH/NF) were also prepared by an *in-situ* growth method, showing greatly enhanced electrocatalytic performances (Table S1).

2. Experimental section

2.1. Chemicals

All the chemicals were purchased from Sinopharm Chemical Reagent Corp. with analytical grade and used without further purification.

2.2. Preparation of ultrathin Ni_3FeAl_x–LDH nanosheets

In a typical procedure, prescribed amounts of $Ni(NO_3)_2{\cdot}6H_2O$, $Fe(NO_3)_3{\cdot}9H_2O$ and $Al(NO_3)_3{\cdot}9H_2O$ were dissolved in 75 mL of mixed deionized water and ethanol (V_{H2O}: V_{EtOH}=9:1) to form a solution with a total metal ion concentration of 2.0 mmol/L. The ratio of Ni^{2+}, Fe^{3+} and Al^{3+} were fixed at 3: 1: x (x=0, 1.0, 1.5 or 3.0). Triethanolamine (TEA) was added into the mixture; the concentration of TEA in the final solution is 3 times higher than the total contents of Fe^{3+} and Al^{3+}. Then 16 mmol of hexamethylenetetramine (HMT) were added into the mixture and stirred for 0.5 h. The solution was transferred into a stainless-steel Teflon-lined autoclave, which was sealed and maintained at 95 °C for 10 h and then cooled down naturally to room temperature. The products were collected by centrifugation at 3000 rpm for 5 min, washed by excessive ethanol and deionized water for several times, and then freeze-dried under vacuum at −40 °C overnight.

2.3. Preparation of Ni_3FeAl_x–LDH/NF electrodes

Typically, a piece of Ni foam (~3 cm×4 cm) was cleaned by subsequent ultrasonication in acetone, ethanol and 6 M HCl solution for 15 min respectively, and then washed by deionized water for 3 times. The cleaned Ni foam was transfer into a stainless-steel Teflon-lined autoclave containing the same precursor solution for preparing Ni_3FeAl_x–LDH nanosheets, and reacted under the same conditions as described above. The as-obtained Ni_3FeAl_x–LDH/NF electrode was washed by deionized water and ethanol for several times, and then freeze-dried for further use.

2.4. Characterizations

The morphology and compositions of these samples were examined by transmission electron microscopy (TEM, JEM-2100), scanning electron microscopy (SEM, Hitachi-S4800) and Energy-dispersive X-ray spectroscope (EDX) attached to the SEM. The crystallinity of products was characterized by X-ray diffraction (XRD) on a Rigaku-Ultima IV powder diffractometer using Cu Kα (λ=1.5418 Å) radiation at scan rate of 10°/min between 10° and90°. X-ray photoelectron spectra (XPS) were obtained using a PHI-5000 VersaProbe X-ray photoelectron spectrometer with an Al Kα X-ray radiation. Inductively coupled plasma optical emission spectrometer (ICP-OES) were carried out using Optima 5300DV analyzer.

2.5. Electrochemical measurements

For preparing electrodes, 5.0 mg of Ni_3FeAl_x–LDH was dispersed into a 1.0 mL of ethanol and deionized water mixed solution ($V_{ethanol}$: V_{H2O}=9:1) containing 40 μL aqueous solution of nafion (5 wt%), and then ultrasonicated for 0.5 h. The mixture was pasted onto a rotating disk electrode (RDE, 5 mm diameter) with a loading mass of 0.2 mg/cm^2. The electrochemical measurements were performed in a three-electrode system connected with an electrochemical workstation (Chenhua CHI-760E). The electrolyte was 1.0 M KOH, the counter electrode was Pt foil, and the reference electrode was Hg/HgO electrode (MMO) filled with 1.0 M KOH. Prior to the tests, high-purity N_2 was bubbled through the electrolyte to eliminate dissolved oxygen. Cyclic voltammetry (CV) was performed for 30 cycles between −0.20 and 0.75 V *vs.* MMO at a scan rate of 300 mV/s to clean the surface of electrode.

To confirm that the Al species in the Ni_3FeAl_x-LDHs were partially etched/dissolved in strong alkaline solution during the electrochemical tests, we also performed EDX analysis on Ni_3FeAl_x-LDH electrodes after electrochemical treatments (CV scanning between −0.20 and 0.75 V *vs.* MMO at a scan rate of 300 mV/s for 30 circles in oxygen-saturated 1.0 M KOH solution, then washing in deionized water and dried at room temperature).

The electrochemical surface area (ECSA) was estimated according to the roughness factor (R_f) [28]. Briefly, CVs were recorded between −0.15 and −0.05 V *vs.* MMO at the scan rates from 5 to 200 mV/s. In this potential range, the current was originated from the electrical double layers rather than the charge transfer reactions of electrode. The current density $\Delta j=(j_a-j_c)$ at −0.10 V *vs.* MMO was plotted against the scan rates, and the slope was the C_{dl}. The R_f ($R_f=C_{dl}/60$ μF/cm^2) was calculated by dividing C_{dl} with the capacitance of smooth metal oxide surface [39].

For OER tests, linear scan voltammogram (LSV) was carried out from −0.20 to 0.75 V *vs.* MMO at a scan rate of 10 mV/s on RDE at 2400 rpm in oxygen-saturated 1.0 M KOH solution to ensure the O_2/H_2O equilibrium at 1.23 V *vs.* RHE. The LSV of Ni_3FeAl_x/NF catalysts was carried out in the potential range from −0.20 to 0.75 V *vs.* MMO at a scan rate of 1 mV/s, with a loading mass of 0.5 mg/cm^2. The activity of Ni_3FeAl_x/NF catalysts was normalized by the geometric area. And the chronopotentiometric measurements were recorded at the current

density of 20 mA/cm^2. All potentials were calibrated with reversible hydrogen electrode (RHE) by the Nernst Eq. (1):

$$E_{RHE}(\mathrm{V}) = E_{MMO} + 0.059pH + E^0_{MMO} = E_{MMO} + 0.059pH + 0.098 \quad (1)$$

and the overpotential was calculated as following:

$$\eta(\mathrm{V}) = E_{MMO} + 0.059pH + E^0_{MMO} - 1.23 = E_{MMO} + 0.059pH + 0.098 - 1.23 \quad (2)$$

The OER Faradaic efficiency over the Ni_3FeAl_x–LDH catalysts was measured by RRDE. Prior to the tests, high-purity N_2 flow was bubbled into 1.0 M KOH electrolyte for 25 min and maintained throughout the experiment to purge the system. The disk potential was held at 0.65 V *vs.* MMO in the OER kinetic-limited region for 2 min, while the ring current was collected at −0.60 V *vs.* MMO. The Faradaic efficiency was determined as below:

$$Faradaic\ efficiency = \frac{n}{N}\cdot\frac{i_r}{i_d} \quad (3)$$

where n is the number of electrons (n=2), N is the collection efficiency of RRDE (N=0.386 in this work), i_r and i_d are the measured ring current and disk current, respectively.

The turnover frequency (TOF) was calculated as following: [40]

$$TOF = \frac{I}{4Fm} \quad (4)$$

where I is the current at 1.58 V *vs.* RHE (with the overpotential of 350 mV), F is the Faraday constant (96485 C/mol), and m is the mole number of the total active material dropped on the glassy carbon electrode.

3. Results and discussion

3.1. Characterizations and OER performances of Ni_3FeAl_x–LDH nanosheets

The experimental process for preparing ultrathin Ni_3FeAl_x–LDH nanosheets (x=0, 0.91, 1.27 or 2.73) is detailed in the Experimental section, as illustrated in Fig. 1a. Transmission electron microscopy (TEM) and scanning electron microscopy (SEM) were employed to investigate the morphology and structure of Ni_3FeAl_x–LDH samples. The TEM images of as-obtained Ni_3FeAl_x–LDH products are shown in Fig. 1b-e, indicating that ultrathin nanosheet structures with size larger than 200 nm have been successfully synthesized. As the Al content increases to higher level, the morphology of Ni_3FeAl_x–LDH nanosheets become more rough and amorphous (Fig. 1c-e), indicating the crystallinity is gradually decreased. Sponge-like nanoporous structures can be found in the $Ni_3FeAl_{1.27}$–LDH and $Ni_3FeAl_{2.73}$–LDH nanosheets (Fig. 1d,e). SEM characterization confirms that the Ni_3Fe–LDH nanosheets are with smooth surface and lamellar structure (Fig. 1f). In accordance with the TEM observations, the SEM images of $Ni_3FeAl_{0.91}$–LDH, $Ni_3FeAl_{1.27}$–LDH and $Ni_3FeAl_{2.73}$–LDH nanosheets (Fig. 1g-i) present more rough and fragmented morphology along with the increase of Al content. The decreased crystallinity was attributed to Al substitution, which increased the structural disorder of Ni_3FeAl_x–LDH nanosheets. The crystalline structures of products were examined by X-ray diffraction spectroscopy (XRD), as shown in Fig. 2a. The XRD peaks of Ni_3FeAl_x–LDH nanosheets can be accordingly ascribed to the Ni_3Fe–LDH phase (JCPDS card No. 51-0463, *R–3m(166): a=b=3.080, c=22.950*). Owing to the introduction of Al species, resulting in lattice distortion, the positions of (003), (006), (012) and (113) peaks slightly shifted, and the full widths at half maximum (FWHM) of above peaks were broaden [9,14]. The XRD results confirmed that the Al substitution changed the interplanar spacings and decreased the crystallization degree of Ni_3FeAl_x–LDH products.

The compositions of Ni_3FeAl_x–LDH nanosheets were examined by X-ray photoelectron spectroscopy (XPS) and energy dispersive X-ray spectroscopy (EDX). The Al contents of Ni_3FeAl_x–LDHs were calculated according to the EDX results (Fig. S1), and the survey spectra of XPS (Fig. S2) are consistent with the EDX analysis. In the high-resolution XPS spectra of Ni_3FeAl_x–LDH nanosheets around Ni 2p region (Fig. 2b–e and Fig. S3a), the main peaks and satellite peaks of $Ni2p_{3/2}$ and $Ni2p_{1/2}$ can be clearly observed. The high-resolution XPS spectra around Fe 2p region are also presented in Figs. S3b and S4. Along with the increasing Al content, the peaks of Ni $2p_{3/2}$ and Ni $2p_{1/2}$ moved to higher energy, while the peaks of Fe $2p_{3/2}$ and Fe $2p_{1/2}$ moved to lower energy. The $Ni2p_{3/2}$ binding energy of Ni_3Fe–LDH, $Ni_3FeAl_{0.91}$–LDH, $Ni_3FeAl_{1.27}$–LDH and $Ni_3FeAl_{2.73}$–LDH nanosheets are about 855.4 eV, 855.6 eV, 855.7 eV and 855.9 eV, respectively. The $Ni2p_{3/2}$ binding energy can be deconvoluted into two peaks at 855.0 eV and 856.1 eV, corresponding to the oxidation states of Ni^{2+} and Ni^{3+}, respectively [41]. In order to reveal the influence of Al content on the valence states of the nickel ions, the percentage of Ni^{3+} in all Ni species (Ni^{3+} and Ni^{2+}) calculated by the XPS results as a function of the atomic ratio of Al^{3+} in all metal atoms ($C(Al^{3+})$) was plotted, as presented in Fig. 3a. As the $C(Al^{3+})$ increased, the proportion of Ni^{3+} in Ni species also increased, suggesting it was increased as a result of a higher level of Al content. However, the atomic ratio of Ni^{3+} in all metal atoms didn't monotonically increase along with the Al content (Fig. 3b). The concentration of Ni^{3+} in $Ni_3FeAl_{0.91}$–LDH (~48.0% of all metal atoms) is the highest among the Ni_3FeAl_x–LDH samples, which is consistent with the electrochemical surface area of the data. The calculated R_f values of $Ni_3FeAl_{0.91}$-LDH was the largest among the samples (Fig. S5). The EDX spectra of Ni_3FeAl_x–LDH samples (Fig. S1) revealed the co-existence of corresponding elements. More accurate information was gathered by using ICP-OES. For this analysis, appropriate samples were dissolved in diluted hydrochloric acid. The content of every metal element in Ni_3FeAl_x–LDH was listed in Table S2.

The electrocatalytic OER activity of Ni_3FeAl_x–LDHs was investigated in 1.0 M KOH with a standard three-electrode system (as detailed in the Experimental section). During OER tests, the working electrode kept a rotating speed of 2400 rpm to remove oxygen bubbles generated by catalysts. Fig. 3c shows the iR-corrected OER polarization curves recorded at a slow scan rate of 10 mV/s to minimize capacitive current. The ECSA of samples was estimated by the roughness factor (R_f) measured from CV curves (Fig. S5). The redox peaks at 1.38–1.48 V (Fig. S6) during the anodic and cathodic scans were resulted from the conversion between Ni^{2+} and Ni^{3+} in alkaline electrolyte. At the current density of 1.0 mA/cm^2, the overpotential of $Ni_3FeAl_{0.91}$–LDH is 300 mV, which is 20 mV lower than that of Ni_3Fe–LDH (320 mV); the overpotential of $Ni_3FeAl_{1.27}$–LDH and $Ni_3FeAl_{2.73}$–LDH are 323 mV and 327 mV, respectively (Fig. 3c). The $Ni_3FeAl_{0.91}$–LDH shows the lowest onset potential, revealing its highest activity for OER. This result is consistent with the previous report that the number of Ni^{3+} and Fe^{3+} active sites can affect the onset potential for OER [32]. Fig. 3c summarized the current densities (red columns) of Ni_3FeAl_x–LDHs at a fixed potential of 1.58 V *vs.* RHE (with overpotential of 350 mV). The current density of $Ni_3FeAl_{0.91}$–LDH nanosheets is 13.2 mA/cm^2, which is 6.6 times higher than that of Ni_3Fe–LDH (2.0 mA/cm^2), and also much higher than $Ni_3FeAl_{1.27}$–LDH (3.36 mA/cm^2) and $Ni_3FeAl_{2.73}$–LDH (2.90 mA/cm^2). Fig. 3d shows the Tafel plots of all samples obtained from polarization curves. The Tafel slopes of $Ni_3FeAl_{0.91}$–LDH (50 mV/dec), $Ni_3FeAl_{1.27}$–LDH (53 mV/dec) and $Ni_3FeAl_{2.73}$–LDH (52 mV/dec) greatly outperformed that of Ni_3Fe–LDH (97 mV/dec), confirming the significantly enhanced OER activity of Ni_3FeAl_x–LDH samples. As shown in Fig. S7, the Faradaic efficiency measured by RRDE was 92.5% for Ni_3Fe–LDH, 97.2% for $Ni_3FeAl_{0.91}$–LDH, 96.7% for $Ni_3FeAl_{1.27}$–LDH and 96.4% for $Ni_3FeAl_{2.73}$–LDH, respectively. The high Faradaic efficiency indicated that the reaction on the disk electrode was mainly OER, rather than the oxidation of catalysts. The TOF of Ni_3FeAl_x–LDH samples was calculated according to Eq. (4).

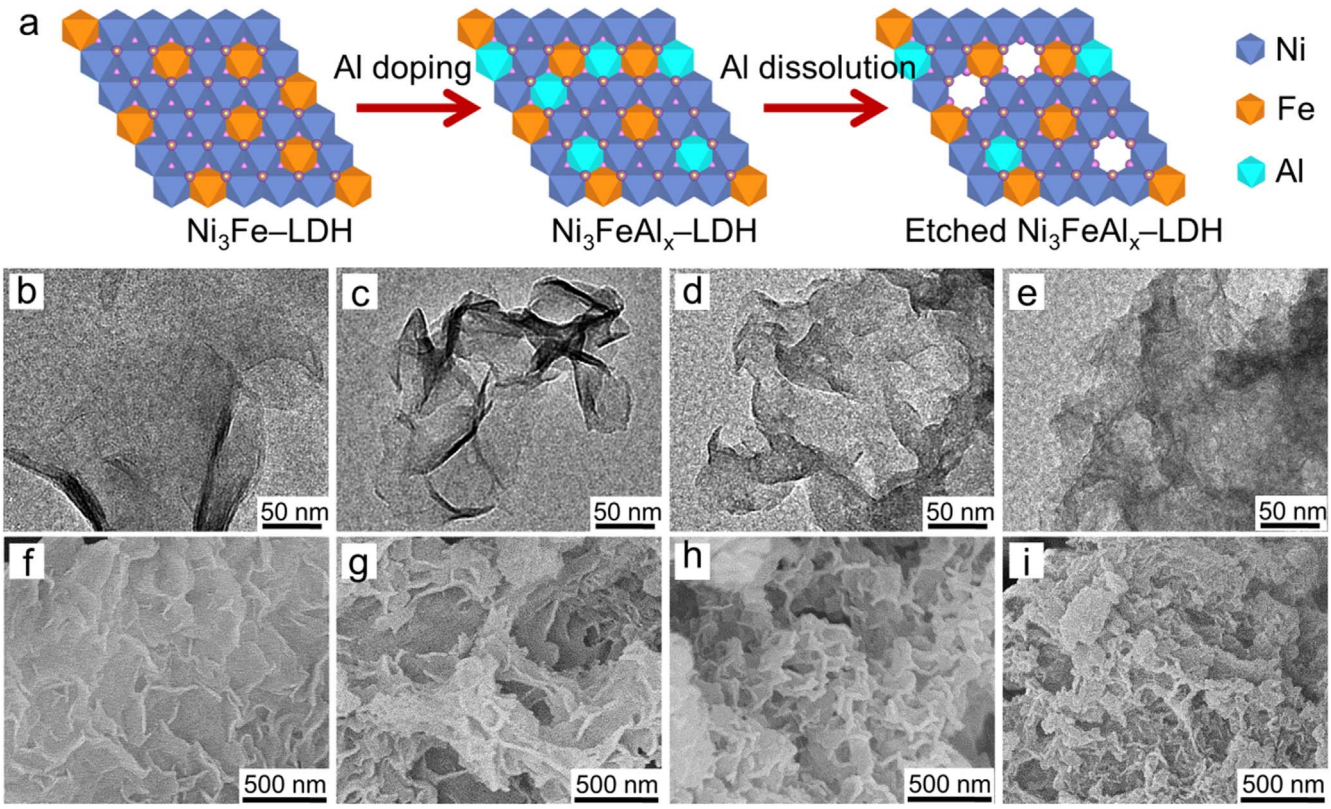

Fig. 1. (a) Schematic preparation of Ni_3FeAl_x–LDH nanosheets, (b-e) TEM and (f-i) SEM images of as prepared ultrathin Ni_3FeAl_x–LDH nanosheets: (b, f) Ni_3Fe–LDH, (c, g) $Ni_3FeAl_{0.91}$–LDH, (d, h) $Ni_3FeAl_{1.27}$–LDH, (e, i) $Ni_3FeAl_{2.73}$–LDH, respectively.

The TOF of the $Ni_3FeAl_{0.91}$–LDH is 0.170 s^{-1}, which is higher than that of $Ni_3FeAl_{1.27}$–LDH (0.040 s^{-1}), $Ni_3FeAl_{2.73}$–LDH (0.030 s^{-1}) and Ni_3Fe–LDH (0.015 s^{-1}), suggesting that $Ni_3FeAl_{0.91}$–LDH has the highest activity for OER.

For comparison, we also measured the compositions of Ni_3FeAl_x–LDH electrodes after electrochemical treatment (CV scanning between −0.20 and 0.75 V at a scan rate of 300 mV/s for 30 circles in oxygen-saturated 1.0 M KOH solution), as shown in Fig. S8. The EDX spectra revealed the percentages of Al element in the Ni_3FeAl_x–LDH nanosheets after electrochemical treatment were greatly reduced, comparing to those of pristine Ni_3FeAl_x–LDH nanosheets (Fig. S1). The results confirmed that the Al species on the surface of Ni_3FeAl_x–LDH nanosheets were partially etched/dissolved in alkaline solution. The high long-term durability and electrochemical stability of Ni_3FeAl_x–LDH nanosheets in alkaline solution was also confirmed by the continuous OER testing of Ni_3FeAl_x–LDH/NF electrodes for 18 h, as detailed in the following section.

Based on the above results, we present the following discussions to fully explicate the electrocatalytic activity improvement originated from Al substitution: (1) From Fig. 3a and b, it can be concluded that the OER activity of Ni_3FeAl_x–LDHs is monotonically related to the content of Ni^{3+}, rather than the content of Al^{3+} or the proportion of Ni^{3+} in all Ni species. Clearly, Fig. 3b demonstrates that both the content of Ni^{3+} and the OER electrocatalytic activity of Ni_3FeAl_x–LDHs show a volcano-type dependence on the content of Al doping. It indicates that the concentration of Ni^{3+} sites on the catalyst surface plays a crucial role in determining the performance of Ni-based LDH electrocatalysts. This is coincident with the previous report [43] that a layer of Ni^{3+} sites (or NiOOH) can be developed on the catalyst surface at potentials approaching the evolution of oxygen and the electrochemical activity of Ni^{3+} sites is very high towards OER. While the Fe doping can also decrease the overpotential and increase the catalytic activity at high potentials for OER [42]. (2) The partial etching/dissolution of Al^{3+} in strong alkaline solution would create more defects in the N_3FeAl_x–LDH lattices [44,45], hence further enlarging the ECSA and R_f. In the process of Al^{3+}dissolution, more Ni and Fe active sites were exposed on the surface of sponge-like and porous N_3FeAl_x–LDH nanosheets, thus the OER catalytic activity was greatly enhanced. This is also in accordance with the previous literature [33,34,46–49] that low-coordinated Ni, Fe and Co sites resulted from defects or vacancies can improve the catalytic activity. In brief, the appropriate ratio of Al element in N_3FeAl_x–LDH nanosheets greatly increased the number of active sites, therefore significantly enhanced the catalytic performance towards OER.

3.2. Characterizations and OER performances of Ni_3FeAl_x–LDH/NF electrodes

The practical application of LDHs as electrode materials was usually hampered by the poor electronic conductivity and slow ion transport. To resolve this problem, we performed the *in-situ* growth of Ni_3FeAl_x–LDH nanosheets on 3D porous and conductive Ni foam, which further led to a dramatic improvement in the electrochemical performance. Fig. 4 show the SEM images of as-prepared Ni_3FeAl_x–LDH/NF electrodes. The resultant ultrathin Ni_3FeAl_x–LDH nanosheets with size of several hundred nanometers were homogeneously grown on Ni foams. As the content of Al element increased, the surface of nanosheets become rougher and more wrinkled, which is consistent with the above characterizations of pristine Ni_3FeAl_x–LDH nanosheets (Fig. 1). Compared to bare Ni foam (Fig. S9), it can be confirmed that the surface of Ni_3FeAl_x–LDH/NF electrodes was completely covered by Ni_3FeAl_x–LDH nanosheets. SEM was performed to investigate the morphology and structure of Ni_3FeAl_x–LDH/NF electrodes after long-term chronopotentiometric OER measurements at the current density of 20 mA/cm^2 in 1.0 M KOH solution for 18 h (Fig. S10). From the SEM images, it can be seen that there is not a significant change in the morphology and structure of Ni_3FeAl_x–LDH/NF electrodes after long-term OER electrolysis and Al^{3+} dissolution; However, the surface

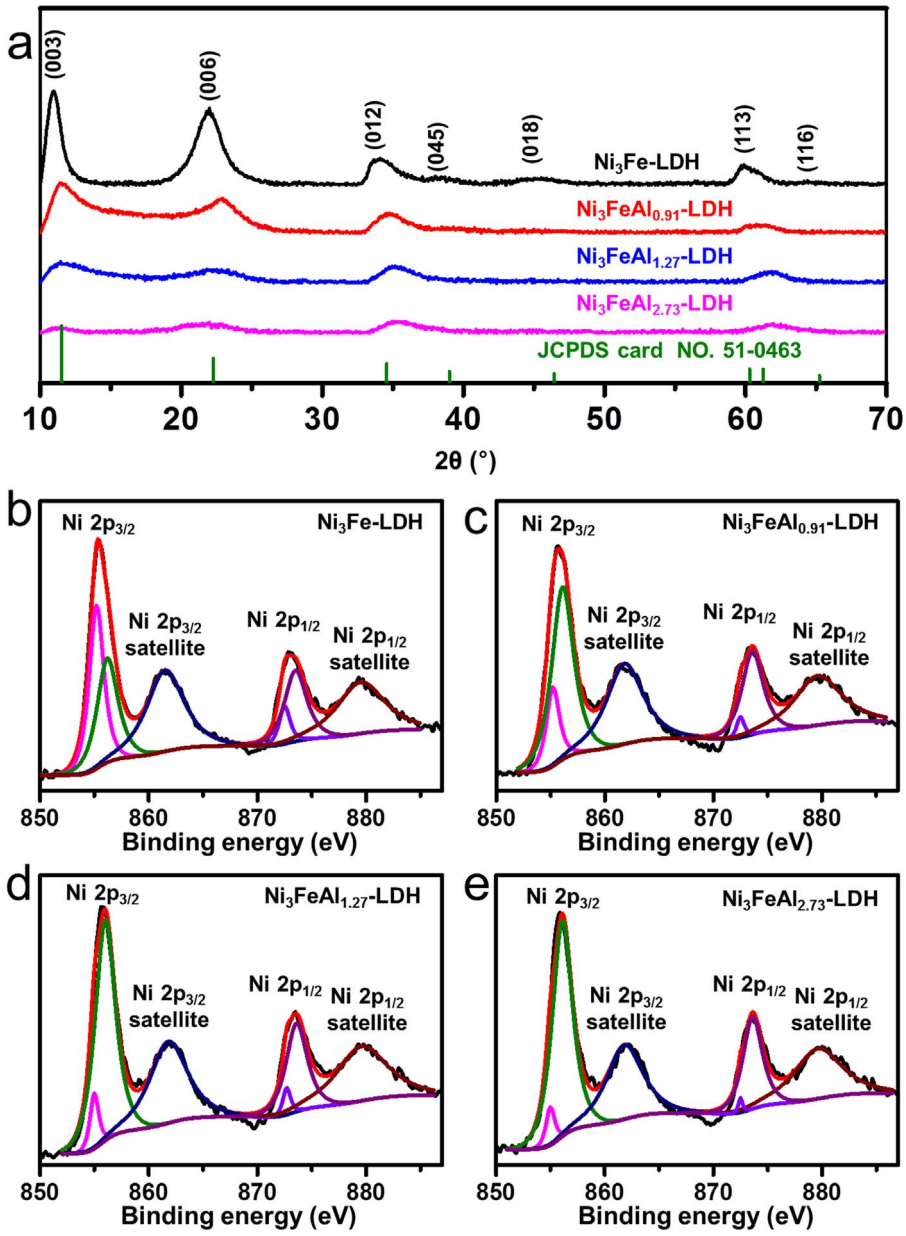

Fig. 2. (a) XRD spectra and (b–e) XPS spectra at Ni 2p region of Ni_3FeAl_x–LDH nanosheets (x=0, 0.91, 1.27 and 2.73, respectively).

became rougher and more porous, indicating more active sites of Ni^{3+} and Fe^{3+} were exposed to the surface, which could be very helpful to the enhancement of OER activity.

The OER performances of Ni_3FeAl_x–LDH/NF products were systematically measured. Fig. 5 shows the electrocatalytic performance of Ni_3FeAl_x–LDH/NF electrodes and pristine Ni foam control sample in 1.0 M KOH solution. Compared to pristine Ni foam, Ni_3FeAl_x–LDH/NF electrodes show remarkably improved catalytic activity (Fig. 5a). The redox peaks at ~1.41 V were resulted from the transformation between $Ni(OH)_2$ and NiOOH ($Ni(OH)_2+OH^- \leftrightarrow NiOOH+H_2O+e^-$) in alkaline electrolyte [40]. Among these 3D-networked electrodes, $Ni_3FeAl_{0.91}$–LDH/NF shows the highest catalytic activity, in accordance with the above results of pristine $Ni_3FeAl_{0.91}$–LDH nanosheets. Besides, the current densities of Ni_3FeAl_x–LDH/NF electrodes are much higher than their counterpart pristine Ni_3FeAl_x–LDH nanosheets without Ni foam, demonstrating the merits of 3D-porous and highly-conductive Ni foam. The overpotentials of all samples at the current density of 20 mA/cm^2 were summarized in Fig. 5b. The overpotential of $Ni_3FeAl_{0.91}$–LDH/NF (304 mV) is lower than Ni_3Fe–LDH/NF (336 mV), $Ni_3FeAl_{1.27}$–LDH/NF (306 mV), $Ni_3FeAl_{2.73}$–LDH/NF (316 mV) and pristine Ni foam (376 mV). At a fixed potential of 1.60 V *vs.* RHE, the current density of $Ni_3FeAl_{0.91}$–LDH nanosheets is 235 mA/cm^2, which is 4.4 times higher than that of Ni_3Fe–LDH (53 mA/cm^2), and also much higher than those of $Ni_3FeAl_{1.27}$–LDH (120 mA/cm^2), $Ni_3FeAl_{2.73}$–LDH (105 mA/cm^2) and pristine Ni foam (20 mA/cm^2). The catalytic activity of the samples at high potentials can be ranked as the following order: $Ni_3FeAl_{0.91}$–LDH/NF > $Ni_3FeAl_{1.27}$–LDH/NF≈$Ni_3FeAl_{2.73}$–LDH/NF > Ni_3Fe–LDH/NF > > pristine Ni foam. Fig. S11 shows the Tafel plots of all samples obtained from the polarization curves (Fig. 5a). The Tafel slopes of $Ni_3FeAl_{0.91}$–LDH/NF, $Ni_3FeAl_{1.27}$–LDH/NF and $Ni_3FeAl_{2.73}$–LDH/NF are 57, 63 and 67 mV/dec, respectively. In contrast, the Tafel slope of Ni_3Fe–LDH/NF is much higher (91 mV/dec), indicating that the Al substitution can greatly improve the OER activity. Besides, the Tafel slopes of Ni_3FeAl_x–LDH/NF electrodes are slightly higher than the electrodes made of powdery Ni_3FeAl_x–LDHs and nafion binder measured by RDE, which is owing to the accumulation of oxygen bubbles on the surface of Ni_3FeAl_x–LDH/NF electrodes.

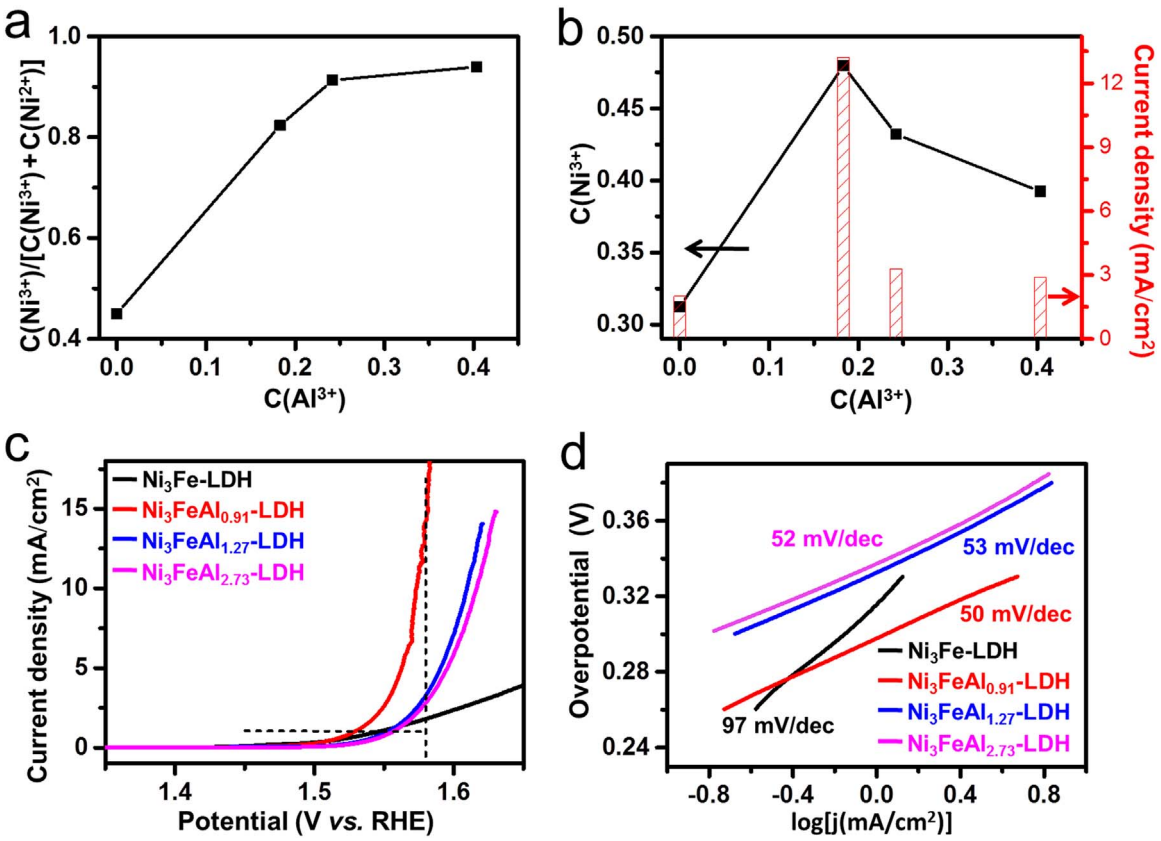

Fig. 3. (a) The percentage of Ni^{3+} in all Ni species (Ni^{3+} and Ni^{2+}) against the atomic ratio of Al^{3+} in all metal atoms of Ni_3FeAl_x–LDH nanosheets (x=0, 0.91, 1.27 or 2.73). (b) The atomic ratio of Ni^{3+}(black dots) and the current density at the potential of 1.58 V *vs.* RHE (red columns) against the atomic ratio of Al^{3+} in all metal atoms of Ni_3FeAl_x–LDH nanosheets. (c) The iR-corrected OER polarization curves and (d) Tafel plots of Ni_3FeAl_x–LDH nanosheets recorded at a scan rate of 10 mV/s in 1.0 M KOH.

Furthermore, the stability of as-prepared catalysts toward OER was also investigated. During the chronopotentiometric tests of the samples at 20 mA/cm^2 (Fig. 5c), there were some fluctuations in overpotential, which were originated from the absorption/accumulation and desorption of oxygen bubbles on the electrode surface. Even so, the overpotentials of Ni_3FeAl_x–LDH/NF electrodes after testing for 18 h

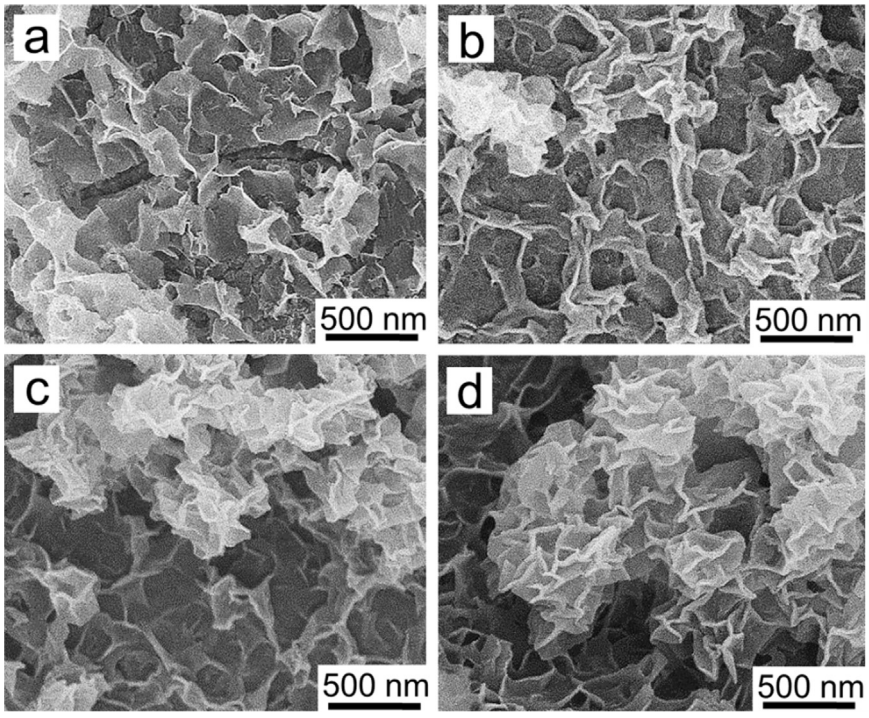

Fig. 4. SEM images of as-obtained Ni_3FeAl_x–LDH nanosheets grown on Ni foams: (a) Ni_3Fe–LDH/NF, (b) $Ni_3FeAl_{0.91}$–LDH/NF, (c) $Ni_3FeAl_{1.27}$–LDH/NF and (d) $Ni_3FeAl_{2.73}$–LDH/NF, respectively.

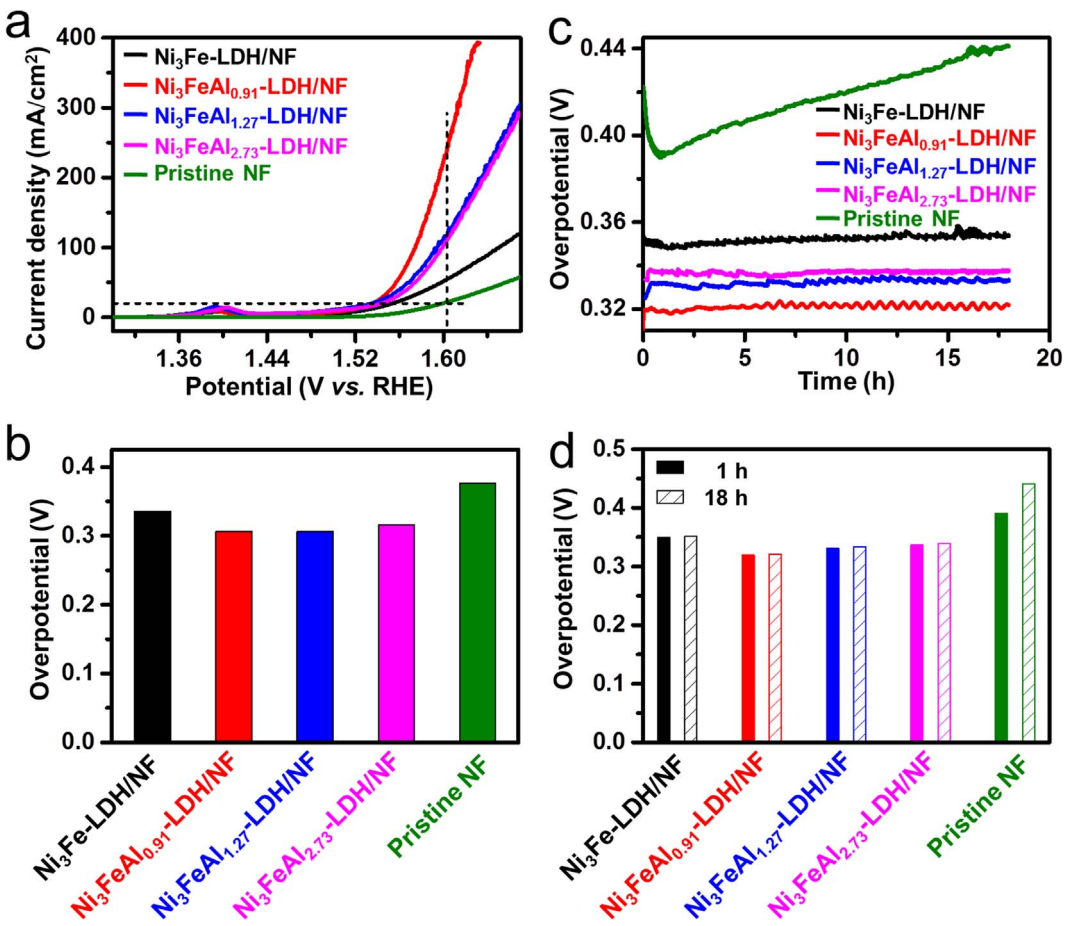

Fig. 5. (a) OER performance of Ni_3Fe–LDH/NF, Ni_3FeAl_x–LDH/NF and pristine Ni foam electrodes recorded at 1.0 mV/s in 1.0 M KOH solution. (b) The overpotentials of above samples obtained from (a) at the current density of 20 mA/cm^2. (c) Chronopotentiometric measurements at the current density of 20 mA/cm^2 in 1.0 M KOH solution. (d) The overpotentials obtained from (c) after continuous testing for 1 h (solid columns) and 18 h (patterned columns).

show no obvious change, in contrast to the sharp activity loss of pristine Ni foam. The overpotentials of all samples after testing for 1 h and 18 h are compared in Fig. 5d. After continuously tested for 18 h, the overpotential of pristine Ni foam increased more than 50 mV, while the overpotentials of Ni_3FeAl_x–LDH/NF electrodes increased only ~3 mV, indicating the high stability of Ni_3FeAl_x–LDH/NF electrodes. It can be concluded that the $Ni_3FeAl_{0.91}$–LDHs/Ni foam electrode shows the best activity and excellent long-term stability, maintaining a stable overpotential of 320 mV at 20 mA/cm^2 after testing for 18 h.

4. Conclusions

In summary, we have introduced Al as the doping element into ultrathin trinary Ni_3FeAl_x-LDH nanosheets, which exhibit greatly-enhanced OER activity than Ni_3Fe-LDH. After the partial dissolution of Al^{3+} species on the catalyst surface, the number of exposed active sites were further increased. Interestingly, both the atomic ratio of Ni^{3+} and the electrocatalytic activity of Ni_3FeAl_x–LDHs presented an identical volcano–type dependence on the contents of Al substitution, indicating that the high concentration of Ni^{3+} active sites on the catalyst surface derived from the appropriate ratio of Al element is a vital factor in determining the OER activity. Moreover, the Ni_3FeAl_x–LDH nanosheets grown on Ni foam showed even higher OER activity, attributing to the highly-porous and 3D-conductive architecture of Ni foam. This study provides a new insight into the role of elemental doping in electrocatalysts. The outstanding features of high activity, favorable kinetics, and prominent durability indicate that Ni_3FeAl_x–LDHs can be used as high-performance catalysts for OER in alkaline medium.

Notes

The authors declare no competing financial interest.

Acknowledgements

This work is supported by National Natural Science Foundation of China (Nos. 21403105 and 21573108), National 973 Basic Research Program (No. 2015CB659300), National Materials Genome Project (2016YFB0700600), China Postdoctoral Science Foundation (Nos. 2015M581775 and 2016M601767), Natural Science Foundation of Jiangsu Province (Nos. BK20150583 and BK20160643), Fundamental Research Funds for the Central Universities and a project funded by the Priority Academic Program Development (PAPD) of Jiangsu Higher Education Institutions.

Appendix A. Supplementary material

Supplementary data associated with this article can be found in the online version at doi:10.1016/j.nanoen.2017.04.011.

References

[1] Y. Matsumoto, E. Sato, Mater. Chem. Phys. 14 (1986) 397–426.
[2] N. Yang, C. Tang, K.Y. Wang, G. Du, A.M. Asiri, X.P. Sun, Nano Res. 9 (2016) 3346–3354.
[3] C. Tang, A.M. Asiri, X.P. Sun, Chem. Commun. 52 (2016) 4529–4532.
[4] C. Tang, N.Y. Cheng, Z.H. Pu, W. Xing, X.P. Sun, Angew. Chem. Int. Ed. 54 (2015) 9351–9355.
[5] N.Y. Cheng, Q. Liu, A.M. Asiri, W. Xing, X.P. Sun, J. Mater. Chem. A 3 (2015)

23207–23212.
[6] K. Zeng, D. Zhang, Prog. Energ. Combust. 36 (2010) 307–326.
[7] G.A. Olah, G.K.S. Prakash, A. Goeppert, J. Am. Chem. Soc. 133 (2011) 12881–12898.
[8] T. Reier, M. Oezaslan, P. Strasser, ACS Catal. 2 (2012) 1765–1772.
[9] Y.E. Roginskaya, T.V. Varlamova, M.D. Goldstein, I.D. Belova, B.S. Galyamov, R.R. Shifrina, V.A. Shepelin, V.N. Fateev, Mater. Chem. Phys. 30 (1991) 101–113.
[10] N. Danilovic, R. Subbaraman, K.C. Chang, S.H. Chang, Y. Kang, J. Snyder, A.P. Paulikas, D. Strmcnik, Y.T. Kim, D. Myers, V.R. Stamenkovic, N.M. Markovic, Angew. Chem. Int. Ed. 53 (2014) 1–7.
[11] D. Friebel, M.W. Louie, M. Bajdich, K.E. Sanwald, Y. Cai, A.M. Wise, M.-J. Cheng, D. Sokaras, T.-C. Weng, R. Alonso-Mori, R.C. Davis, J.R. Bargar, J.K. Nørskov, A. Nilsson, A.T. Bell, J. Am. Chem. Soc. 137 (2015) 1305–1313.
[12] J. Huang, J. Chen, T. Yao, J. He, S. Jiang, Z. Sun, Q. Liu, W. Cheng, F. Hu, Y. Jiang, Z. Pan, S. Wei, Angew. Chem. Int. Ed. 54 (2015) 1–7.
[13] Z. Lu, L. Qian, Y. Tian, Y. Li, X. Sun, X. Duan, Chem. Commun. 52 (2016) 908–911.
[14] F. Song, X.L. Hu, Nat. Commun. 5 (2014) 4477.
[15] X.M. Zhou, Z.M. Xia, Z.Y. Zhang, Y.Y. Ma, Y.Q. Qu, J. Mater. Chem. A 2 (2014) 11799–11806.
[16] J.W. Nai, H.J. Yin, T.T. You, L.R. Zheng, J. Zhang, P.X. Wang, Z. Jin, Y. Tian, J.Z. Liu, Z.Y. Tang, L. Guo, Adv. Energy Mater. 5 (2015) 1401880.
[17] F. Song, X. Hu, J. Am. Chem. Soc. 136 (2014) 16481–16484.
[18] L. Qian, Z. Lu, T. Xu, X. Wu, Y. Tian, Y. Li, Z. Huo, X. Sun, X. Duan, Adv. Energy Mater. 5 (2015) 1500245.
[19] O. Diaz-Morales, I. Ledezma-Yanez, M.T.M. Koper, F. Calle-Vallejo, ACS Catal. 5 (2015) 5380–5387.
[20] M.W. Loui, A.T. Bell, J. Am. Chem. Soc. 135 (2013) 12329–12337.
[21] K. Yan, T. Lafleur, J. Chai, C. Jarvis, Electrochem. Commun. 62 (2016) 24–28.
[22] M. Gong, Y. Li, H. Wang, Y. Liang, J.Z. Wu, J. Zhou, J. Wang, T. Regier, F. Wei, H. Dai, J. Am. Chem. Soc. 135 (2013) 8452–8455.
[23] J. Luo, J.-H. Im, M.T. Mayer, M. Schreier, M.K. Nazeeruddin, N.-G. Park, S.D. Tilley, H.J. Fan, M. Grätzel, Science 345 (2014) 1593–1596.
[24] A.S. Batchellor, S.W. Boettcher, ACS Catal. 5 (2015) 6680–6689.
[25] X.M. Li, X.G. Hao, Z.D. Wang, A. Abudula, G.Q. Guan, J. Power Sources 347 (2017) 193–200.
[26] W.W. Xu, Z.Y. Lu, P.B. Wan, Y. Kuang, X.M. Sun, Small 12 (2016) 2492–2498.
[27] L. Trotochaud, S.L. Young, J.K. Ranney, S.W. Boettcher, J. Am. Chem. Soc. 136 (2014) 6744–6753.
[28] S. Chen, J. Duan, P. Bian, Y. Tang, R. Zheng, S.-Z. Qiao, Adv. Energy Mater. 5 (2015) 1500936.
[29] J. Jiang, A. Zhang, L. Li, L. Ai, J. Power Sources 278 (2015) 445–451.
[30] C. Tang, H.-S. Wang, H.-F. Wang, Q. Zhang, G.-L. Tian, J.-Q. Nie, F. Wei, Adv. Mater. 27 (2015) 4516–4522.
[31] Y. Jia, L.Z. Zhang, G.P. Gao, H. Chen, B. Wang, J.Z. Zhou, M.T. Soo, M. Hong, X.C. Yan, G.R. Qian, J. Zou, A.J. Du, X.D. Yao, Adv. Mater. (2017) 1700017–1700024.
[32] Y. Hou, M.R. Lohe, J. Zhang, S.H. Liu, X.D. Zhuang, X.L. Feng, Energy Environ. Sci. 9 (2016) 478–483.
[33] K. Xu, P. Chen, X. Li, Y. Tong, H. Ding, X. Wu, W. Chu, Z. Peng, C. Wu, Y. Xie, J. Am. Chem. Soc. 137 (2015) 4119–4125.
[34] A. Bergmann, E. Martinez-Moreno, D. Teschner, P. Chernev, M. Gliech, J.F. de Araujo, T. Reier, H. Dau, P. Strasser, Nat. Commun. 6 (2015) 8625.
[35] J.H. Wang, W. Cui, Q. Liu, Z.C. Xing, A.M. Asiri, X.P. Sun, Adv. Mater. 28 (2016) 215–230.
[36] J.L. Lado, X. Wang, E. Paz, E. Carbó-Argibay, N. Guldris, C. Rodríguez-Abreu, L. Liu, K. Kovnir, Y.V. Kolen'ko, ACS Catal. 5 (2015) 6503–6508.
[37] C. Tang, R. Zhang, W.B. Lu, L.B. He, X.E. Jiang, A.M. Asiri, X.P. Sun, Adv. Mater. 29 (2017) 1602441–1602446.
[38] S. Koh, P. Strasser, J. Am. Chem. Soc. 129 (2007) 12624–12625.
[39] B. Lu, D. Cao, P. Wang, G. Wang, Y. Gao, Int. J. Hydrog. Energy 36 (2011) 72–78.
[40)] Y. Qiu, L. Xin, W. Li, Langmuir 30 (2014) 7893–7901.
[41] A.P. Grosvenor, M.C. Biesinger, R.S.C. Smart, N.S. McIntyre, Surf. Sci. 600 (2006) 1771–1779.
[42] Y.F. Li, A. Selloni, ACS Catal. 4 (2014) 1148–1153.
[43] B.S. Yeo, A.T. Bell, J. Power Sources 116 (2012) 8394–8400.
[44] T. Xu, X. Wu, Y. Li, W. Xu, Z. Lu, Y. Li, X. Lei, X. Sun, Chem. Electro Chem. 2 (2015) 679–683.
[45] B. Wang, G.R. Williams, Z. Chang, M. Jiang, J. Liu, X. Lei, X. Sun, ACS Appl. Mater. Interfaces 6 (2014) 16304–16311.
[46] J.Y.C. Chen, L.N. Dang, H.F. Liang, W.L. Bi, J.B. Gerken, S. Jin, E.E. Alp, S.S. Stahl, J. Am. Chem. Soc. 137 (2015) 15090–15093.
[47] D.A. Corrigan, J. Electrochem. Soc. 134 (1987) 377–384.
[48] J. Landon, E. Demeter, N. İnoğlu, C. Keturakis, I.E. Wachs, R. Vasić, A.I. Frenkel, J.R. Kitchin, ACS Catal. 2 (2012) 1793–1801.
[49] X.H. Li, F.C. Walsh, D. Pletcher, Phys. Chem. Chem. Phys. 13 (2011) 1162–1167.